Experimental Study on Impact and Deposition Behaviours of Multiple Surges of Channelized Debris Flow on a Flexible Barrier

By

Dao-Yuan TAN
Department of Civil and Environmental Engineering
The Hong Kong Polytechnic University, Hung Hom, Kowloon, Hong Kong, China
Email: rztdy2009@gmail.com

Jian-Hua YIN (Chair Professor and Corresponding Author)
Department of Civil and Environmental Engineering
The Hong Kong Polytechnic University, Hung Hom, Kowloon, Hong Kong, China
Tel: (852) 2766-6065, Fax: (852) 2334-6389, Email: cejhyin@polyu.edu.hk

Jie-Qiong QIN
Department of Civil and Environmental Engineering
The Hong Kong Polytechnic University, Hung Hom, Kowloon, Hong Kong, China
Email: jieqiong.qin@connect.polyu.hk

Zhuo-Hui ZHU
Department of Civil and Environmental Engineering
The Hong Kong Polytechnic University, Hung Hom, Kowloon, Hong Kong, China
Email: zhuo-hui.zhu@connect.polyu.hk

and

Wei-Qiang FENG
Department of Civil and Environmental Engineering,
The Hong Kong Polytechnic University, Hung Hom, Kowloon, Hong Kong. China
Email: fengweiqiang2015@gmail.com

Manuscript submitted to *Landslides* for possible publication as an Original Paper

October 2019

Abstract

Debris flow normally occurs after heavy rains in mountainous regions with multiple surges. Flexible barriers are installed in torrents to intercept debris flows in an early stage. For the safer design of a flexible barrier installed in the upstream, the forces on the barrier invaded by debris flows should be taken into consideration. An outdoor physical modelling facility was utilized to study the interaction between debris flows and a flexible barrier. Three continuous debris flow impact tests were conducted to investigate the performance of a flexible barrier affected and overflowed by multiple surges of debris flow. A parameter named Initial Block Ratio (IBR) is introduced in this study to describe the initial condition of a flexible barrier filled by the earlier debris flow surges. By analysing the results of these tests, the dynamic response of a flexible barrier under the impact of multiple surges of debris flow is studied, and the influence of IBR on the interaction of debris flow with the flexible barrier is investigated. Based on the findings of the experimental study, a new simple method is proposed to calculate the loads on a filled flexible barrier overflowed by debris flow. By comparing with the measured impact force in the overflow test, this method has a good performance and can be utilized in design analysis with further calibration.

Keywords: multiple surges of debris flow; flexible barrier; physical model; impact force; simple method

1. Introduction

In a natural gully with a large amount of loose sediment, large-amplitude, regularly repeating debris-flow surges occasionally occur under heavy rains (Xu et al. 2012; Yagi et al. 2009; Zanuttigh and Lamberti 2007; Chen et al. 2017; McCoy et al. 2010). Kean et al. (2013) concluded based on the observations of two field sites that large-amplitude regularly repeating surges could occur under the rain intensity larger than 30 mm/hr. Those debris flows carry large boulders and tree trunks, which impose a threat to human lives and infrastructure (Su et al. 2017; Cui et al. 2018). Alternatively, multi-level barrier systems are utilized to retain debris material with the advantages of increasing the retaining volume and reducing the dynamic impact loading progressively (WSL 2008; Shum and Lam 2011; Ng. et al. 2017; Glassey 2013). Flexible barriers have been increasingly used to mitigate debris flows by arresting major components (debris, boulders, and tree trunks) and dewatering debris material to weaken the mobility (Volkwein et al. 2011; Wendeler et al. 2018; Kwan et al. 2014). Multi-level flexible barriers have been placed in Europe for intercepting channelized debris flows (Wendeler et al. 2008; Volkwein et al. 2011). In a multi-level barrier system, the upstream barriers installed in the triggering areas are designed to be overflowed by a large-scale debris flow which normally contains multiple debris surges (Glassey 2013; Ng. et al. 2017). A few studies have considered flow-structure interaction for the multiple-barrier system. Choi et al. (2014) investigated dry granular flow impacting multiple baffle rows using flume experiments. Ng. et al. (2017) studied the interaction of the dual-barrier system with a dry granular flow using physical modelling tests. They concluded that the upstream barrier could reduce the impact pressure on the downstream barrier due to momentum redirection and flow-thinning. Volkwein et al. (2011) explored the loading situation of a filled flexible barrier being overflowed based on field observation. The dynamic response of a flexible barrier impacted, filled, and overflowed by multiple debris flow surges requires further research.

The aim of this paper is to study the performance of a flexible barrier impacted and overflowed by multiple debris flow surges and provide suggestions for the design of debris-resisting flexible barriers which are allowed to be overflowed. Physical modelling is utilized by many researchers in the study of geohazard initiation and mitigation (Wendeler 2016; Paik et al. 2012; Cui et al. 2017). Scaling plays a crucial role in experiment design aimed at studying the behaviours of debris flow and landslide (Iverson 2015). Artificial debris flows generated in physical modelling experiments are difficult to reach the same scale as real debris flow events. Even for the large-scale physical modelling facility built by USGS with a debris capacity of 10 m^3 and a flume length of 95 m (Iverson et al. 1992), the flow depth and the Froude number of the generated debris flows were different from real events (Hungr et al. 1984; Costa 1984; Iverson et al. 2010). Geotechnical centrifuge has been utilized to investigate the initiation and flow mechanisms of debris flows by reproducing the field-scale stress states (Kailey et al. 2011; Bowman et al. 2010; Turnbull et al. 2015). However, for the study on the dynamic response of a flexible barrier under debris flow impacts, a scale model is difficult to realistically reflect the dynamic behaviour of different components of a full-scale flexible barrier (Wendeler et al. 2018). As an alternative, physical modelling experiments utilizing a field-scale flexible barrier are conducted in this study. Debris flows are generated in an outdoor modelling facility with the kinetic energies and impact forces comparable to real debris flow events, which are sufficient for studying the dynamic response of a flexible barrier under the impact of a debris flow. The environment and key variables in physical modelling experiments can be well controlled, and the experiment data can be collected by the systematic arrangement of instrumentation. In this study, a series of physical modelling tests are performed using an outdoor physical modelling facility to quantitatively investigate the impact behaviours of multiple debris flow surges and their interactions within a flexible barrier. Three debris flow surges are generated with the interval of one week to study the successive impacts of multiple debris flow surges. The dynamic response of the flexible barrier under the impact of multiple surges and the deposition behaviors of the debris flow surges arriving at different times are presented and analysed in this study. Based on the findings from those tests, a new simple method is proposed to estimate the forces on a filled flexible barrier overflowed by a debris flow surge. A comparison with the measured impact force in the overflow test validates this newly proposed simple method.

2. Description of the physical modelling facility

A physical modelling testing facility was built in an outdoor experiment site of the Hong Kong Polytechnic University. This facility consists of three main components (see Figure 1): (i) a reservoir with a capacity of 5 m^3, (ii) a replaceable instrumented commercial flexible barrier with a width of 2.48 m and a height of 1.48 m, and (iii) a steel flume with a width of 1.5 m, a length of 7 m and an inclination of 35° to accelerate the generated debris flows. The reservoir has a vent and a flip-up door facing the flume to store debris material and initiate debris flows. The flexible barrier is supported by two inclined posts, and each post is supported by two inclined strand cables. The posts are hinged to the foundations and can rotate freely in the direction of debris flow impact to transmit the impact force to the supporting strand cables. The flexible barrier is made up of steel wire rings with a diameter of 300 mm (No. ROCCO 7/3/300, Geobrugg).

Those components and structures have been commonly used in Hong Kong and Europe for geo-hazards mitigation (Wendeler 2016; Ng. et al. 2012). Details of the physical modelling facility were given in our previous study (Tan et al. 2018b). In this study, a secondary wire mesh net with a mesh size of 50 mm was utilized to retain coarse particles (coarse aggregate particles in this study have the diameters ranging from 20 to 50 mm) and allow slurry and small particles pass through. Sidewalls of the flume are made up of tempered glass to provide a clear observation of the moving debris flow and its interaction with the flexible barrier.

Instrumentation

The instrumentation arrangement of the physical model is plotted in Figure 2. Tension link transducers with the capacity of 50 kN are installed on the supporting strand cables. A data-logger (model name NI PXIe-1082, National Instruments) capable of sampling 48 transducers at 1000 Hz simultaneously is used to collect the data of all transducers. Two high-speed cameras (model name MacroVis EoSens, HSVISION) with the resolution of 1024×768 pixels and the sampling rate of 1000 f/s are utilized to measure the velocity of the debris flow before impact and capture the interaction between the debris flow and the flexible barrier. One high-speed camera is located at the right side of the barrier, and the other one is placed in front of the barrier, as illustrated in Figure 2.

3. Experiment material and procedures

The debris material was prepared by mixing Completely Decomposed Granite (CDG) and aggregate with water using an electronic soil mixer before being poured into the reservoir. The coarse aggregate content of the debris material used in the tests was managed referring to the Tsing Shan debris flow in Hong Kong (King 2013) to reflect the particle size distribution (PSD) characteristics in a debris flow event. As a comparison, The PSD curves of the debris materials used in this study and the Tsing Shan debris flow are plotted in Figure 3. The percentage of coarse particles (diameter larger than 10 mm) is similar to the debris flow event as a reference. Three successive tests were conducted with the time interval of one week to study the dynamic response of a flexible barrier impacted and filled by multiple debris flow surges. The measured parameters of the debris flows in the tests are listed in Table 1. Because of the small retaining ratio of the flexible barrier in Test 1, two adjustments were made for higher trapping ratios in the following experiments. In Debris Tests 2 and 3, the debris volumes were increased, and more coarse particles were added in the debris mixture, which led to an increase of the coarse fraction and a decrease of the water content. The procedures of one test are described as follows: at the beginning of the test, the door is flipped up in less than 0.5 s with the help of a mechanical door-opening system. This door-opening system is composed of a pair of levels as the lock of the door and four tensile springs to assist the door opening progress. A detailed introduction of this system was given in the literature (Tan et al. 2018b). Then, the data-logger starts to record data several minutes before initiation of debris flow to obtain the initial values of the transducers. The high-speed cameras capture the motion of the debris flow and its interaction with the flexible barrier by loop recording, and the recording is triggered to stop at the end of the test. The depth and velocity of the approaching debris front before impact are measured from continuous photographs by the side-view high-speed camera, as listed in Table 1. There are limitations to this measurement method. First, the flume boundary may cause eddies of the flow whose velocity cannot be accurately measured from the side view. Second, the flow depth at the center of the flume can be lower than that at the two sides due to continuous flow thinning in an accelerating slope. To increase the accuracy of the measurement, two actions are taken: first, the location and the shooting angle of the side-view high-speed camera are selected to be perpendicular to the sidewall of the flume by overlapping two posts in the photographs ; second, the velocity of the debris flow is averaging from the velocities of five individual particles measured from five continuous photographs before impact with the assistance of the reference lines attached to the flume. The starting time of the impact in each test is set to 0 second, while the negative values indicate the times before impact. In the side-view photographs, the motions of several selected particles are traced and plotted by vectors to represent the moving and impact characteristics of the debris flow.

4. Test result analysis

Multiple debris flow impact tests with overflow

The flexible barrier before each test was blocked gradually by the deposited debris materials in the previous tests (see Figure 4). The interactions of multiple debris flow surges with the flexible barrier are investigated with the help of the high-speed photographs and the measured impact forces. By comparing the impact behaviours of the debris flow surges and the dynamic responses of the flexible barrier in Debris Tests 1-3, how the initial condition of the flexible barrier affects the impact characteristics of debris flow is studied.

Initial conditions of the flexible barrier in the debris flow impact tests

The photographs illustrating the initial conditions of the flexible barrier in Debris Tests 1, 2 and 3 are plotted in Figure 4. The initial block areas in Debris Tests 2 and 3 were measured before each test as A_{block}. For Debris Test 1, the flexible barrier was empty before the test and A_{block} is 0. To quantify the initial blockage of the flexible barrier, a parameter is defined as the Initial Block Ratio (IBR):

$$IBR = \frac{A_{block}}{A_{impact}} \tag{1}$$

where A_{impact} is the total impact area of the debris flow, which is equal to the cross-sectional area of the flume width multiplied by the flexible barrier height. The Initial Block Ratios of Debris Tests 1, 2, and 3 are 0, 0.44 and 0.78 as presented in Figure 5.

Impact force estimation and analysis

The impact force on the supporting structures is calculated from the measured tensile forces on the strand cables using the equation delivered in Tan et al. (2018a):

$$F_{Cables,equivalent} = \frac{l_{post}}{l_{impact}} \left[(F_{BL} + F_{BR}) \cdot \cos\delta \cdot \cos\beta - (F_{AL} + F_{AR}) \cdot \cos\gamma \cdot \cos\alpha \right] \tag{2}$$

where $F_{Cables,equivalent}$ is the equivalent impact force on the supporting structures, l_{post} is the distance between the rotation fulcrum of the post and the connecting point of the cables, l_{impact} is the distance between the rotation fulcrum of the post and the equivalent impact height of the debris flow, F_{AL}, F_{AR}, F_{BL}, and F_{BR} are the measured tensile forces on different supporting cables, where “L” and “R” denote “Left” and “Right”, α, β, γ, and δ are the included angles between the cables and the impact direction, as listed in Figure 2. For the facility used in this study, α is 62°, β is 24°, γ is 76°, and δ is 60°.

Results of the debris flow tests with different initial IBRs

Impact force-time history of the flexible barrier

The accumulated impact forces on the supporting structures are plotted in Figure 6. Since the interval between two tests is one week due to the long preparation period, it is difficult to continuously monitor the forces on the flexible barrier for the three tests. As a compromise, the static force finally recorded in the previous test is considered as the initial load from the trapped debris flow on the flexible barrier in the following test. The peak of the dynamic impact force occurred at the beginning of the impact in Debris Test 1, followed by an oscillating impact loading and a static earth pressure. The oscillating response is attributed to the elastic deformation of the flexible barrier under the dynamic impact of the debris flow. After the impact process, the trapped debris material with the mass of only hundreds of kilograms and the flexible barrier composed an oscillating system. The static earth pressure after impact decreased gradually due to dewatering and pore-pressure dissipation of the debris deposition, which may affect the calculation of the incremented impact force in the following test. The static earth pressure in each test was recorded until the signal was stable. In Debris Test 1, the dynamic impact loading and the static earth pressure are relatively low compared to the other two tests. In Debris Test 2, the impact force increases gradually during the impact process, drops from the loading peak, and keeps stable afterward, which is similar to the tests performed in the literature (Wendeler et al. 2018; Ashwood and Hungr 2016; Song et al. 2019). The gradual increase of the impact loading indicates that the static earth pressure due to debris material deposition plays a key role in the test. In Debris Test 3, an instant impact peak, a consecutive dynamic impact loading lasting 1.5 s, and a stable static earth pressure coexist in the overflow process. The magnitude of the incremented impact force in Debris Test 3 is the largest among the series of tests. Beside the different impact mechanisms which can affect the impact forces on the flexible barrier in the three tests, various debris volumes and water contents in the tests may also affect the impact forces.

Impact behaviour of Debris Test 1 with IBR of 0

The flexible barrier before Debris Test 1 was empty. Thus, the IBR value in this test was 0. The impact process of Debris Test 1 is plotted in Figure 7 by high-speed photographs. A certain percentage of small particles and slurry passed through the flexible barrier with a residual velocity. In fact, only 10% of the debris material was trapped by the flexible barrier, which led to a relatively low impact force on the flexible barrier among the tests (see Figure 6).

Impact behaviour of Debris Test 2 with IBR of 0.44

The flexible barrier before Debris Test 2 was partially blocked by the trapped debris material in Debris Test 1 (see Figure 4b). Based on the above definition, the Initial Block Ratio (IBR) of Debris Test 2 was 0.44. The impact process in Debris Test 2 is plotted in Figure 8 by high-speed photographs. Due to the delayed triggering of the high-speed cameras, the recording time started at 0.78 s. A certain percentage of the debris material was trapped by the flexible barrier during the interaction. At the end of the test, the deposited debris material filled the flexible barrier as a wedge with the deposition height nearly equal to the height of the deformed flexible barrier. From the measurement of the retained debris material volume, nearly 45% of the debris material was trapped by the flexible barrier, which caused that 78% of the flexible barrier was blocked. The impact force on the flexible barrier increased gradually and kept stable afterward (refer to Figure 6), which is similar to the centrifuge debris flow impact tests described in Song et al. (2019). They concluded that the gradually increased impact force and the static load were attributed to the formation of the dead zone, which has also been observed in Debris Test 2 (see the formation of the debris deposition wedge in Figure 8). In analogy with the impact behaviour of the debris flow presented in the literature, the impact force in Debris Test 2 mainly comes from the static earth pressure of the gradual deposition of the trapped debris material. It can be observed from Figure 6 that the maximum impact loading in Debris Test 2 is much larger than Debris Test 1 despite a 10 % difference in total volume and slight differences in PSD as well as impact velocity.

Impact behaviour of Debris Test 3 with IBR of 0.78

Figure 4c shows that the flexible barrier was almost filled by the debris deposition wedge before Debris Test 3, and the mesh net in the impact area was almost fully blocked. In Debris Test 3 (see Figure 9), the debris flow shot up via the top surface of the deposition wedge and overflew the flexible barrier at the beginning of the impact instead of passing through the net (like Debris Test 1) or being trapped (like Debris Test 2). From the side-view photographs in Figure 9, almost no deformation of the flexible barrier occurred in the impact process. Thus, we deduced that the flexibility of the flexible barrier has been seriously jeopardized by the debris deposition trapped in the flexible barrier. Some researchers considered the loading situation in the overflow scenario as a combination of the drag force from the overtopping debris flow and the static earth pressure of the debris deposition (Kwan and Cheung 2012; Volkwein 2014). However, from the force-time history in the overflow stage (see Debris Test 3 in Figure 6), three force components are identified in this study: an instant impact loading, an impact thrust lasting almost 1.5 s, and a static loading. The largest impact force combination occurred at the beginning of the impact. From Figure 9, the debris flow shot up and changed the moving direction at the beginning of the impact process, which imposed a dynamic impact on the flexible barrier. The momentum redirection was also observed by Ng. et al. (2017) in the study of the dual-barrier system impacted by a dry granular flow. By comparing the force-time history with the high-speed photographs, the instant impact loading comes from the debris flow redirection, the impact thrust lasting 1.5 s originates from the drag force between the overflowing debris flow and the debris deposition, and the static loading is attributable to the earth pressure of the debris deposition.

Influence of initial conditions on impact and deposition behaviours

For Debris Test 1, the flexible barrier was empty (IBR=0). In this test, slurry and small particles passed through the flexible barrier, and the flexible barrier deformed obviously under the impact of the debris flow surge. The passing-through of slurry and the large deformation of the flexible barrier led to relatively low dynamic impact loading and static earth pressure from the debris flow. In Debris Test 2, nearly half of the mesh net was blocked by the trapped debris in the previous test (IBR=0.44). In this test, 45% of the debris material was trapped by the flexible barrier, and no obvious passing-through of debris flow was observed in this test. Different debris trapping ratios in Debris Test 1 (10%) and Debris Test 2 (45%) indicate that the initial block ratio of a flexible barrier can obviously affect the deposition behaviour of debris flow. The flexible barrier before Debris Test 3 was almost filled by the trapped debris material in the previous tests. In Debris Test 3, the debris flow climbed up the deposition wedge and overflew the flexible barrier. From the impact force-time history plotted in Figure 6, the largest impact force occurred in the overflow stage (Debris Test 3). Song et al. (2019) compared the impacts from a debris flow on rigid and flexible barriers and found that the impact force on a flexible barrier had a much lower peak loading. They attributed the impact force reduction to the extension of the impact duration in the debris flow-flexible barrier interaction. The peak loads on the flexible barrier could be attenuated by up to 50% due to the large deflection of the flexible barrier based on the study using centrifuge tests (Song et al. 2018). In this study, the jeopardized flexibility and permeability of the flexible barrier by the previous debris flow surges could also be the main reason that the largest dynamic impact force occurred in Debris Test 3 (overflow stage). Under this circumstance, the loading situation in the overflow stage should be considered in the design analysis of debris flow-resisting flexible barriers which are allowed to be overtopped (*e.g.* upstream barriers in a multiple debris-resisting flexible barrier system). We also find that the IBR (Initial Block Ratio) of the barrier can affect the impact characteristics and the peak impact forces by comparing the impact forces of debris flows impacting on a flexible barrier with different initial blockage areas. For the maintenance of debris flow-resisting flexible barriers, the barrier should be cleaned in time after the occurrence of a debris flow event. Even a small-scale debris flow can block a certain part of the barrier and weaken the capability of the flexible barrier in mitigating new debris flows.

5. Calculation of the impact force in the overflow stage

By analyzing the impact characteristics in Debris Test 3, the peak impact load on the flexible barrier in the overflow stage (F_{peak}) can be divided into three force components, which consists of the static earth pressure from the debris deposition (F_{static}), the drag force from the overtopping debris flow (F_{drag}), and the instant peak loading due to momentum redirection ($F_{instant}$):

$$F_{peak} = F_{static} + F_{instant} + F_{drag} \quad (3)$$

In the above equation, the static force (F_{static}) can be calculated using the earth pressure theory, which was first proposed by Armanini (1997) and further developed by Wendeler (2008). According to this method, the impact force is calculated as:

$$F_{static} = 0.5\kappa\rho_{bulk} g h_{deposit}^2 w \quad (4)$$

where $h_{deposit}$ is the total deposition height of the debris flow, w denotes the channel width (m), and κ is the earth pressure coefficient. For rigid barriers, Lichtenan (1973) proposed a range of values between 2.8 and 4.4, while Scotton and Deganutti (1997) suggested the range between 2.5 and 7.5. For flexible barriers, a reduced static coefficient of 1.0 was suggested by Kwan and Cheung (2012) and Wendeler et al. (2018).

The Voellmy model was first proposed to calculate the rheological properties of snow avalanches (Voellmy 1955; Yifru 2014). This model has been widely applied to back-analyse the runout distance and the velocity of the debris flow (Ayotte et al. 1999; Rickenmann et al. 2006; Naef et al. 2006; Bertolo and Wieczorek 2005; Hussin et al. 2012). This model was also suggested to calculate the drag force (F_{drag}) in the overflow stage (Kwan and Cheung 2012). In the Voellmy model, the shear stress between two layers can be calculated by the combination of a frictional term and a turbulent term:

$$\tau = h\rho_{bulk} g \left(\tan\varphi + \frac{v^2}{h\xi} \right) \quad (5)$$

where g is the gravity acceleration, v, h and ρ_{bulk} are the velocity, the height, and the bulk density of the debris flow respectively, φ and ξ are the friction angle and the turbulence coefficient of the debris flow, Hungr (1998) suggested to use φ=11° and ζ=500 m/s^2 for channelized debris flows based on the back analysis of debris flow events in Hong Kong.

The effective area of the drag force is simply estimated by multiplying the top length of the deposition wedge with the width of the channel (Kwan and Cheung 2012). Thus, the drag force can be calculated using the following equation:

$$F_{drag} = h\rho_{bulk} g \left[\tan\varphi + \frac{v^2}{h\xi} \right] \cdot \frac{c_{reduced} \cdot h_{design} \cdot w}{\sin\delta} \tag{6}$$

In this equation, the deposition angle (δ) is an important parameter. From the sketch of the overflow stage plotted in Figure 10a, the deposition angle is the combination of the slope inclination (δ_{slope}) in the retention area and the sedimentation angle (δ_{sed}) of the trapped debris material, which can be written as:

$$\delta = \delta_{slope} + \delta_{sed} \tag{7}$$

In this study, the deposition angle (δ) is 40°, which is measured from the photograph by the side-view camera in the overflow stage (see Figure 10a). The designed flume inclination of the physical modelling facility is 35°, thus the sedimentation angle in the overflow stage is 5°. Kwan and Cheung (2012) suggested 10° for the design analysis of debris flow-resisting flexible barrier, which was obtained by the back-analysis of debris flow events. Considering the various sedimentation angles of different debris materials, the conservative value of 10° is also selected in this study for design analysis.

Another coefficient named $c_{reduced}$ is defined in this study to represent the height reduction ratio of the filled flexible barrier. Wendeler et al. (2018) concluded from field experiments that the filled height of the flexible barrier is 0.75 time of the original height before the event. From the observation of the physical modelling experiments in this study, the height of the filled flexible barrier is 0.6 time of the design height (h_{design}). Due to the initial slack of the flexible barrier by its self-weight, the height of the installed flexible barrier is normally shorter than the design height on the drawings. Thus, $c_{reduced} = 0.6$ (reduced from the design drawing) measured in this study and $c_{reduced} = 0.75$ (reduced from the installed flexible barrier) suggested by Wendeler et al. (2018) are both reasonable. The estimated reduction coefficient $c_{reduced} = 0.6$ from the findings of the physical modelling experiments is selected in the calculation because this value can be easily obtained based on the design drawing of a flexible barrier.

By analysing the impact behavior of the debris flow in Debris Test 3, we conclude that the instant loading mainly comes from the momentum redirection of the debris flow. Based on the impulse-momentum theorem, a simple method is derived to estimate the instant loading. Following the hypotheses made by Armanini (1997) in the derivation of the hydro-dynamic method, two assumptions are made in the calculation:

(a) The debris flow is an incompressible homogeneous continuous medium travelling with a uniform velocity v_0 and a uniform cross-sectional area, which is a rectangle with the width of the channel w and the height of the debris flow h;

(b) Based on the continuum mechanics, the speed and the height of the debris flow before and after momentum redirection are constant.

Thus, the mass of the debris flow (m) can be calculated as:

$$m = t_{instant} v h w \rho_{bulk} \tag{8}$$

where $t_{instant}$ is the duration of the instant loading, v_0 is the impact velocity of the debris flow, ρ_{bulk} is the bulk density of the debris flow, h and w are the height of the debris flow and the width of the channel.

Based on the impulse-momentum theorem and the momentum redirection during the impact (see Figure 10a):

$$F_{instant} t_{instant} = mv - mv \cdot \cos\delta + mv_0 \cdot \sin\delta \tag{9}$$

Substituting Eq.(8) into Eq.(9), $t_{instant}$ in both sides can be eliminated, thus:

$$F_{instant} = v^2 h w \rho_{bulk} (1 - \cos\delta + \sin\delta) \tag{10}$$

Substituting Eq.(4), Eq.(6), and Eq.(10) into Eq.(3), the peak impact force in the overflow stage can be calculated as follows:

$$F_{peak} = 0.5\kappa\rho_d g \left(c_{reduced} h_{design}\right)^2 w + v^2 h w \rho_{bulk} (1 - \cos\delta + \sin\delta) + h\rho_{bulk} g \left[\tan\varphi + \frac{v^2}{h\xi}\right] \cdot \frac{c_{reduced} \cdot h_{design} \cdot w}{\sin\delta} \tag{11}$$

Debris fronts reaching the flexible barrier at different times may have different combinations of debris depths, velocities, and densities (Kwan and Cheung 2012, Wendeler et al. 2018). To be reasonably conservative in the design, the maximum values of those parameters should be used in the impact force calculation.

Tan et al. (2018a) concluded from physical modelling tests that the force transmitted to the supporting structures was much lower than the impact force on the flexible barrier. Therefore, the calculated impact force on the supporting structures should be reduced correspondingly by introducing the Impact Residual Ratio (IRR, β). This value is defined to quantify the ratio of the impact force transmitted from the flexible barrier to the supporting structures as:

$$\beta = \frac{F_{support}}{F_{barrier}} \tag{12}$$

The impact loading on the supporting structures (including the supporting posts, the supporting strand cables, and the foundations) in the overflow stage can be estimated using the following equation:

$$\begin{aligned} F_{peak,s} &= F_{static,s} + F_{instant,s} + F_{drag,s} = 0.5\beta\kappa\rho_d g \left(c_{reduced} \cdot h_{design}\right)^2 w \\ &+ \beta v^2 hw\rho_{bulk}(1-\cos\delta + \sin\delta) + \beta h\rho_{bulk} g\left[\tan\varphi + \frac{v^2}{h\xi}\right] \cdot \frac{c_{reduced} \cdot h_{design} \cdot w}{\sin\delta} \end{aligned} \tag{13}$$

The IRR value (β) can be determined from the results of the dry granular flow impact tests using the same physical modelling facility (Tan et al. 2018a). In that study, around 30% of the impact force from the granular flow was attenuated by the large deformation of the flexible barrier. Thus, 0.7 is selected in this study as the IRR value. The measured force-time history on the supporting structures in the overflow stage (see Figure 6) is used to verify the proposed simple method in this study. The force components on the supporting structures: $F_{static,s}$, $F_{drag,s}$, and $F_{instant,s}$ in Eq.(13) are calculated separately using the parameters listed in Table 2, while the calculated forces are listed in Table 3.

The newly proposed simple method containing three force components, the simple method proposed by Kwan and Cheung (2012) containing the drag force ($F_{drag,s}$) and the static earth pressure ($F_{static,s}$), and the simple method proposed by Wendeler et al. (2018) containing the vertical stress of the overflowing material (σ) and the static earth pressure ($F_{static,s}$) are compared in this study. The comparison results are plotted in Figure 10b. From this comparison, the measured peak impact force at the time of 23 s

($F_{measured,peak}$) fits well with the combination of the force components($F_{static,s} + F_{instant,s} + F_{drag,s}$), and the simple methods in the literature underestimate the maximum impact force. Afterwards, the impact thrust lasting 1.5 s (from 23.2 s to 24.7 s) is underestimated by the force combination of $F_{static,s} + F_{drag,s}$. The underestimation is due to the reason that the turbulence parameters used in the calculation of the drag force are predefined following the suggestions of Hungr (1998), which may not be suitable for the calculation of the debris material used in this study. However, the static earth pressure from the debris deposition is accurately estimated by the hydro-static method ($F_{static,s}$) using the density of the debris deposition (ρ_d), which is measured from the debris material trapped in the flexible barrier after the test. From the comparison results, the simple method can feasibly predict the peak impact force ($F_{measured,peak}$) and the static earth pressure in the overflow stage. Moreover, the parameters in this simple method are predefined or can be easily measured. Therefore, this method can be practically applied in the design of flexible barriers to determine the design impact loading in the overflow stage.

6. Conclusions

The performance of a flexible barrier impacted and overflowed by multiple debris flow surges (Debris Tests 1, 2, 3) was studied using an outdoor physical modelling facility with a well-established data collection system. A parameter named IBR (Initial Block Ratio) was defined to quantify the proportion of the blocked area of a flexible barrier before impact. For the flexible barrier with different IBRs, the impact and deposition characteristics of debris flows were captured and analysed. Among those tests, the debris flow in Debris Test 3 overflowed the flexible barrier *via* the top surface of the debris deposition wedge formed in the previous tests. Three force components were identified from the measured loads on the supporting structures in the overflow stage. A simple method was proposed to calculate the maximum impact force in the overflow stage. This method was verified by the force-time history of the supporting structures. From the experiment data and their analysis, key findings and conclusions are summarized and presented as below:

(a) With the increase of the Initial Block Ratio (IBR), the trapping ratio of the debris material increased correspondingly. In this study, the trapping ratio increased from 10% in Debris Test 1 (IBR=0) to 45% in Debris Test 2 (IBR=0.44).

(b) Before Debris Test 1, the flexible barrier was empty initially (IBR=0). The dynamic impact force acting on the flexible barrier was much smaller than the dynamic impacts in Debris Tests 2 and 3 because a large percentage of debris material passed through the flexible barrier.

(c) Before Debris Test 2, the flexible barrier was partially blocked by the debris deposition in Debris Test 1 (IBR=0.44). A large percentage of debris material was trapped by the flexible barrier in Debris Test 2. The impact force in this test gradually increased with the increment of the debris deposition.

(d) Before Debris Test 3, the flexible barrier was almost filled by the debris deposition in the previous tests (IBR=0.78). Thus, most debris overflowed the flexible barrier *via* the top surface of the deposition wedge. From the force-time history of the supporting structures in the overflow stage, three force components were identified: the drag force from the overtopping debris flow, the impact force from the debris flow redirection, and the static earth pressure from the debris deposition.

(e) A simple method was proposed to estimate the impact force in the overflow stage by calculating the force components with corresponding equations. By comparing with the force-time history of the supporting structures in the overflow stage, the proposed simple method can accurately predict the loads in the overflow stage with simple parameters and coefficients.

From the findings in this study, we suggest that the flexible barrier should be cleaned frequently to keep its capability in preventing debris flows. For an upstream debris flow-resisting flexible barrier in a multi-level flexible barrier system that is allowed to be overflowed, the force situation in the overflow stage could be the severest and should be considered in the design analysis. The new simple method proposed in this study has a great potential for being adopted in the design analysis because all parameters in this simple method have specific physical meanings that have been predefined in this study or can be determined easily. At present, there are still some restrictions on implementing this method. Wendeler and Volkwein (2015) concluded from laboratory tests that the ratio of the mesh size to the particle diameter can affect the retaining rate and the impact force in the interaction of a debris flow with a flexible barrier. Choi et al. (2019) found that the basal clearance of a barrier can obviously reduce the impact forces from a granular flow. While the influences of the mesh size and the basal clearance have not been covered in this study. The definition of IBR (Initial Block Ratio) simplifies the blockage zone, which is normally a 3D deposition wedge, into a 2D blockage area on the flexible barrier. For the debris flows with different debris materials and the natural slopes with different angles of inclination, the shapes of the deposition wedges could be various. Besides, the coefficients suggested by Hungr (1998) for impact force calculation are based on the back analysis of debris flow events in Hong Kong. For the design analysis in other countries and regions, further calibrations of the coefficients are needed for higher prediction accuracy. Considering the importance and complexity of the interaction between a debris flow and a flexible barrier, researches should be progressively conducted to provide more reliable explanations and update the existing guidelines in order to define a more rational design procedure of flexible barriers for mitigating debris flows.

Acknowledgement

The work in this paper is supported by grants (1-BBAG, 1-ZVEH, 3-RBCE, 4-BCAW, 5-ZDAF, G-YN97, B-Q43L, B-Q55N) from The Hong Kong Polytechnic University, China. We also acknowledge the supports by a CRF project (Grant No.: PolyU12/CRF/13E) from Research Grants Council (RGC) of Hong Kong Special Administrative Region Government of China, and Research Institute for Sustainable Urban Development of The Hong Kong Polytechnic University (PolyU), Center for Urban Geohazard and Mitigation of Faculty of Construction and Environment of PolyU, and Geotechnical Engineering Office of the Civil Engineering and Development Department of the Government of the Hong Kong Special Administrative Region.

References

Armanini, A. (1997). On the dynamic impact of debris flows. In *Recent developments on debris flows.* Springer, Berlin, Heidelberg, 208-226.

Ashwood, W., and Hungr, O. (2016). Estimating total resisting force in flexible barrier impacted by a granular avalanche using physical and numerical modeling. *Canadian Geotechnical Journal*, 53(10), 1700-1717.

Ayotte, D., Evans, N., and Hungr, O. (1999). Runout analysis of debris flows and avalanches in Hong Kong. In Proceedings, Slope Stability and Landslides, *Vancouver Geotechnical Society Symposium*, 39-46.

Bertolo, P., and Wieczorek, G. F. (2005). Calibration of numerical models for small debris flows in Yosemite Valley, California, USA. *Natural Hazards and Earth System Sciences*, 5(6), 993-1001.

Bowman, E. T., Laue, J., Imre, B., and Springman, S. M. (2010). Experimental modelling of debris flow behaviour using a geotechnical centrifuge. *Canadian geotechnical journal*, 47(7), 742-762.

Chen, H. X., Zhang, L. M., Gao, L., Yuan, Q., Lu, T., Xiang, B., and Zhuang, W. L. (2017). Simulation of interactions among multiple debris flows. *Landslides*, 14(2), 595-615.

Choi, C. E., Ng, C. W. W., Liu, H., and Wang, Y. (2019). Interaction between Dry Granular Flow and Rigid Barrier with Basal Clearance: Analytical and Physical Modelling. *Canadian Geotechnical Journal*, (ja).

Choi, C. E., Ng, C. W. W., Song, D., Kwan, J. H. S., Shiu, H. Y. K., Ho, K. K. S., and Koo, R. C. H. (2014). Flume investigation of landslide debris–resisting baffles. *Canadian Geotechnical Journal*, *51*(5), 540-553.

Costa, J. E. (1984). Physical geomorphology of debris flows. In *Developments and applications of geomorphology* (pp. 268-317). Springer, Berlin, Heidelberg.

Cui, Y. F., Choi, C. E., Liu, L. H., and Ng, C. W. (2018). Effects of particle size of mono-disperse granular flows impacting a rigid barrier. *Natural Hazards*, *91*(3), 1179-1201.

Cui, Y. F., Zhou, X. J., and Guo, C. X. (2017). Experimental study on the moving characteristics of fine grains in wide grading unconsolidated soil under heavy rainfall. *Journal of Mountain Science*. 14(3), 417-431.

Glassey, T. (2013). *Hydrology and check dams analysis in the debris flow context of Illgraben torrent*. MAS practical research project, Swiss Federal Institute of Technology Zurich, Zurich, Switzerland.

Hungr, O. (1998). Mobility of Landslide Debris in Hong Kong: Pilot Back Analyses using a Numerical Model. *Report prepared for the Geotechnical Engineering Office*, Hong Kong, 50p.

Hungr, O., Morgan, G. C., and Kellerhals, R. (1984). Quantitative analysis of debris torrent hazard for design of remedial measures, *Canadian Geotechnical Journal*, 21, 663–667.

Hussin, H. Y., Quan, L. B., Van Westen, C. J., Christen, M., Malet, J. P., and van Asch, T. W. (2012). Parameterization of a numerical 2-D debris flow model with entrainment: a case study of the Faucon catchment, Southern French Alps. *Natural Hazards and Earth System Sciences*, 12, 3075-3090, https://doi.org/10.5194/nhess-12-3075-2012.

Iverson, R. M. (2015). Scaling and design of landslide and debris-flow experiments. *Geomorphology*, 244, 9-20. Iverson, R. M., Costa, J. E., and LaHusen, R. G. (1992). *Debris-flow flume at HJ Andrews experimental forest, Oregon*. US Geological Survey, Dept. of the Interior.

Iverson, R. M., Logan, M., LaHusen, R. G., and Berti, M. (2010). The perfect debris flow? Aggregated results from 28 large-scale experiments. *Journal of Geophysical Research*, 115, F03005 (Art. No.).

Kailey, P., Bowman, E. T.*, Laue, J., and Springman, S. M. (2011). Modelling debris flow processes with a geotechnical centrifuge. *Italian Journal of Engineering Geology and Environment*, 3, 339-349.

Kean, J. W., McCoy, S. W., Tucker, G. E., Staley, D. M., and Coe, J. A. (2013). Runoff-generated debris flows: Observations and modeling of surge initiation, magnitude, and frequency. *Journal of Geophysical Research: Earth Surface*, 118(4), 2190-2207.

King, J. P. (2013). *Tsing Shan debris flow and debris flood (GEO Report 281*). Geotechnical Engineering Office, HKSAR, 268p.

Kwan, J. S. H., and Cheung, R. W. M. (2012). *Suggestion on design approaches for flexible debris-resisting barriers. Discussion Note DN1/2012.* The Government of Hong Kong Standards and Testing Division, Hong Kong, China.

Kwan, J. S., Chan, S. L., Cheuk, J. C., and Koo, R. C. H. (2014). A case study on an open hillside landslide impacting on a flexible rockfall barrier at Jordan Valley, Hong Kong. *Landslides*, 11(6), 1037-1050.

McCoy, S. W., Kean, J. W., Coe, J. A., Staley, D. M., Wasklewicz, T. A., and Tucker, G. E. (2010). Evolution of a natural debris flow: In situ measurements of flow dynamics, video imagery, and terrestrial laser scanning. *Geology*, *38*(8), 735-738.

Naef, D., Rickenmann, D., Rutschmann, P., and McArdell, B. W. (2006). Comparison of flow resistance relations for debris flows using a one-dimensional finite element simulation model. *Natural Hazards and Earth System Sciences*, 6(1), 155-165.

Ng, A.K.L., Williamson, S.J., and Chong, A.K.T. (2012). Developments in Design Considerations and Use of Flexible Barriers as Mitigation Measures for Channelised Debris Flow and Open Hillslope Failures - A Case Study. In *Proceedings of the One Day Seminar on Natural Terrain Hazard Mitigation Measures.* At Kowloon, Hong Kong.

Ng, C. W. W., Choi, C. E., Koo, R. C. H., Goodwin, G. R., Song, D., and Kwan, J. S. H. (2017). Dry granular flow interaction with dual-barrier systems. *Géotechnique*, 68(5), 386-399.

Paik, J., Son, S., Kim, T., and Kim, S. (2012). A real-scale field experiment of debris flow for investigating its deposition and entrainment. In *AGU Fall Meeting Abstracts*.

Rickenmann, D., Laigle, D. M. B. W., McArdell, B. W., and Hübl, J. (2006). Comparison of 2D debris-flow simulation models with field events. *Computational Geosciences*, 10(2), 241-264.

Scotton, P., and Deganutti, A. M. (1997). Phreatic line and dynamic impact in laboratory debris flow experiments. In *Debris-Flow Hazards Mitigation: Mechanics, Prediction, and Assessment*, 777-786.

Shum, L. K. W. and Lam, A. Y. T. (2011). *Review of natural terrain landslide risk management practice and mitigation measures*, Technical Note TN 3/2011. Hong Kong, China: Geotechnical Engineering Office, Civil Engineering and Development Department, The HKSAR Government.

Song, D., Choi, C. E., Ng, C. W. W., and Zhou, G. G. D. (2018). Geophysical flows impacting a flexible barrier: effects of solid-fluid interaction. *Landslides*, 15(1), 99-110.

Song, D., Zhou, G. G., Xu, M., Choi, C. E., Li, S., and Zheng, Y. (2019). Quantitative analysis of debris-flow flexible barrier capacity from momentum and energy perspectives. *Engineering Geology*, *251*, 81-92.

Su, L.J., Xu, X.Q., Genge, X.Y., and Liang, S.Q. (2017). An integrated geophysical approach for investigating hydro-geological characteristics of a debris landslide in the Wenchuan Earthquake Area. *Engineering Geology*, 219: 52-63, DOI: 10.1016/j.enggeo.2016.11.020

Tan, D. Y., Yin, J. H., Feng, W. Q., Qin, J. Q., and Zhu, Z. H. (2018a). Large-scale physical modelling study of a flexible barrier under the impact of granular flows. *Natural Hazards and Earth System Sciences.*, 18, 2625-2640, https://doi.org/10.5194/nhess-18-2625-2018.

Tan, D. Y., Yin, J. H., Qin, J. Q., Zhu, Z. H., and Feng, W. Q. (2018b). Large-scale physical modeling study on the interaction between rockfall and flexible barrier. *Landslides*, 15(12), 2487–2497.

Turnbull, B., Bowman, E. T., and McElwaine, J. N. (2015). Debris flows: experiments and modelling. Comptes Rendus Physique, 16(1), 86-96.

Voellmy, A. (1955). Uber die Zerstorungskraft von Lawinen. *Schweizerische Bauzeitung, Jahrg.*, 73, 159-162.

Volkwein, A. (2014). *Flexible debris flow barriers. Design and application.* WSL Berichte. Issue 18, 29.

Volkwein, A., Wendeler, C., and Guasti, G. (2011). Design of flexible debris flow barriers. In *5th International Conference debris-flow hazard mitigation. Mechanics, prediction and assessment. Padua, Italy*, 1093-1100.

Volkwein, A., Wendeler, C., and Guasti, G. (2011). Design of Flexible debris flow barriers. *Italian Journal of Engineering Geology and Environment*.

Wendeler, C. (2008). *Murgangrückhalt in Wildbächen: Grundlagen zu Planung und Berechnung von flexiblen Barrieren* (Doctoral dissertation), ETH, Zurich.

Wendeler, C. (2016). *Debris-flow protection systems for mountain torrents: basics principles for planning and calculation of flexible barriers*. WSL Berichte. 44, 281.Wendeler, C., McArdell, B., Volkwein, A., Denk, M., and Gröner, E. (2008). Debris flow mitigation with flexible ring net barriers—field tests and case studies. WIT Trans Eng Sci, 60, 23-31.

Wendeler, C., and Volkwein, A. (2015). Laboratory tests for the optimization of mesh size for flexible debris-flow barriers. *Natural Hazards and Earth System Sciences Discussions*, 3(3).

Wendeler, C., Volkwein, A., McArdell, B. W., and Bartelt, P. (2018). Load model for designing flexible steel barriers for debris flow mitigation. *Canadian Geotechnical Journal*, 99 1-39.

WSL (Swiss Federal Institute for Snow and Avalanche Research) (2008). *Integral risk management of extremely rapid mass movements*. Birmensdorf, Switzerland: WSL.

Xu, Q., Zhang, S., Li, W. L., and Van Asch, T. W. (2012). The 13 August 2010 catastrophic debris flows after the 2008 Wenchuan earthquake, China. *Natural Hazards and Earth System Sciences*, 12, 201-216.

Yagi, H., Sato, G., Higaki, D., Yamamoto, M., and Yamasaki, T. (2009). Distribution and characteristics of landslides induced by the Iwate–Miyagi Nairiku Earthquake in 2008 in Tohoku District, Northeast Japan. *Landslides*, 6(4), 335.

Yifru, A. L. (2014). *Assessment of rheological models for run-out distance modeling of sensitive clay slides, focusing on Voellmy rheology* (master's thesis). Norwegian University of Science and Technology, Trondheim, Norway.

Zanuttigh, B., and Lamberti, A. (2007). Instability and surge development in debris flows. *Reviews of Geophysics*, *45*(3).

Figure List:

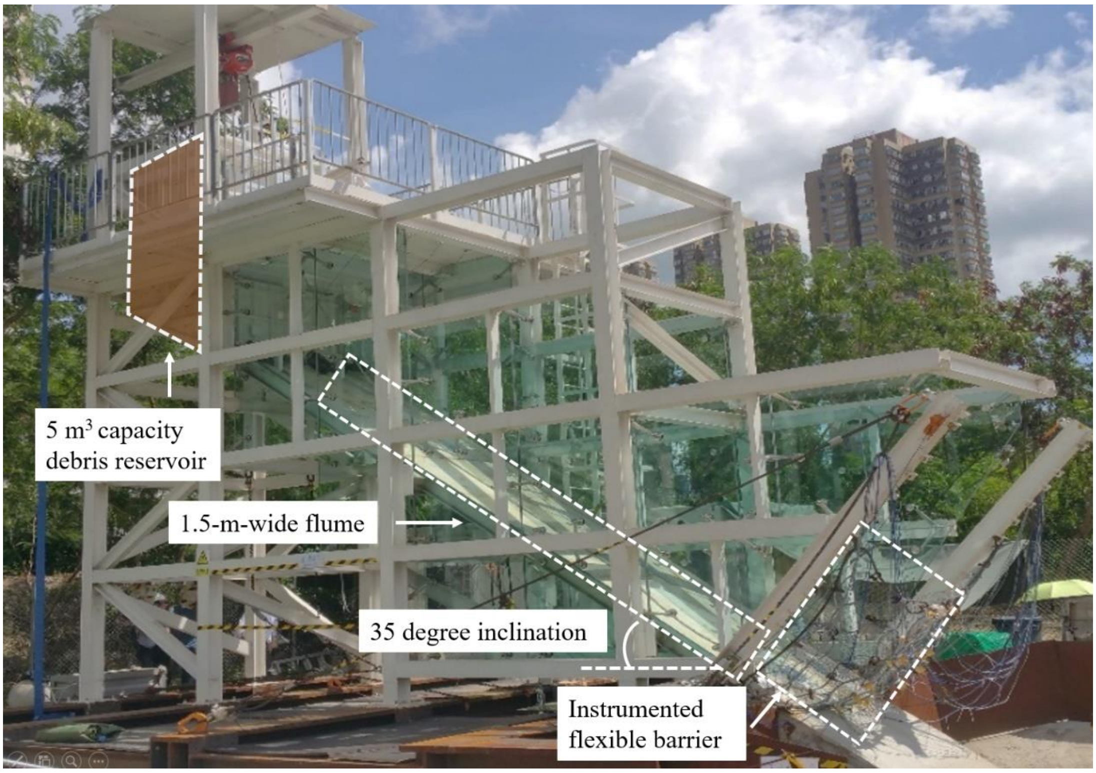

Figure 1. Photo of the large-scale physical model

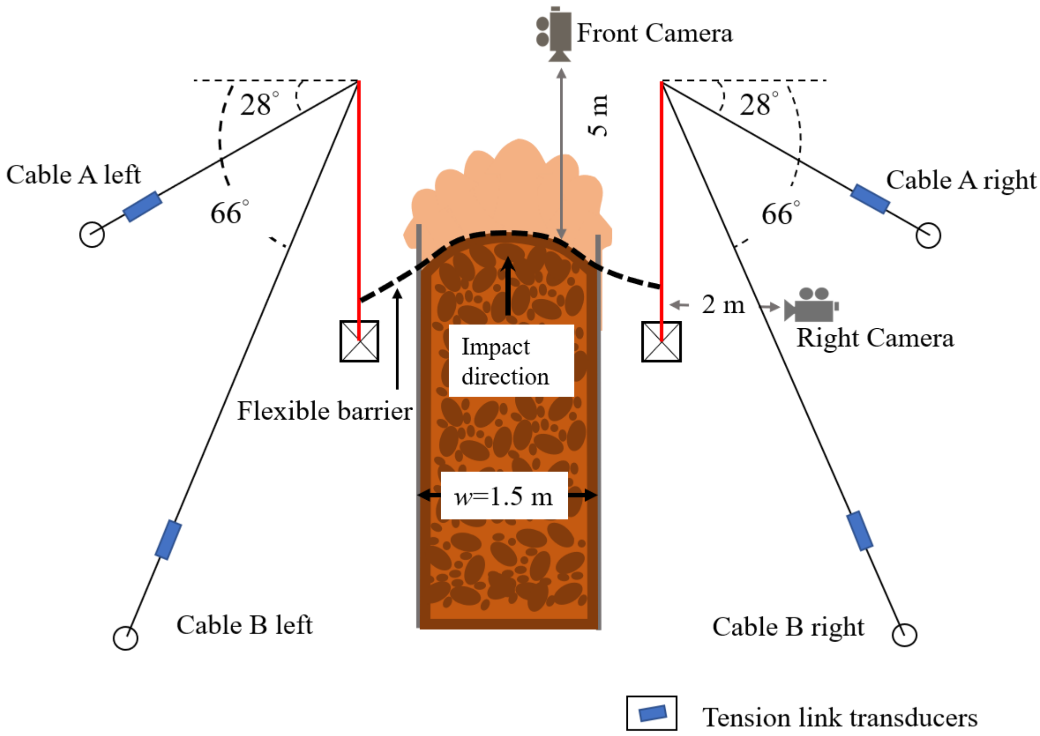

Figure 2. Instrumentation of the outdoor physical modelling facility

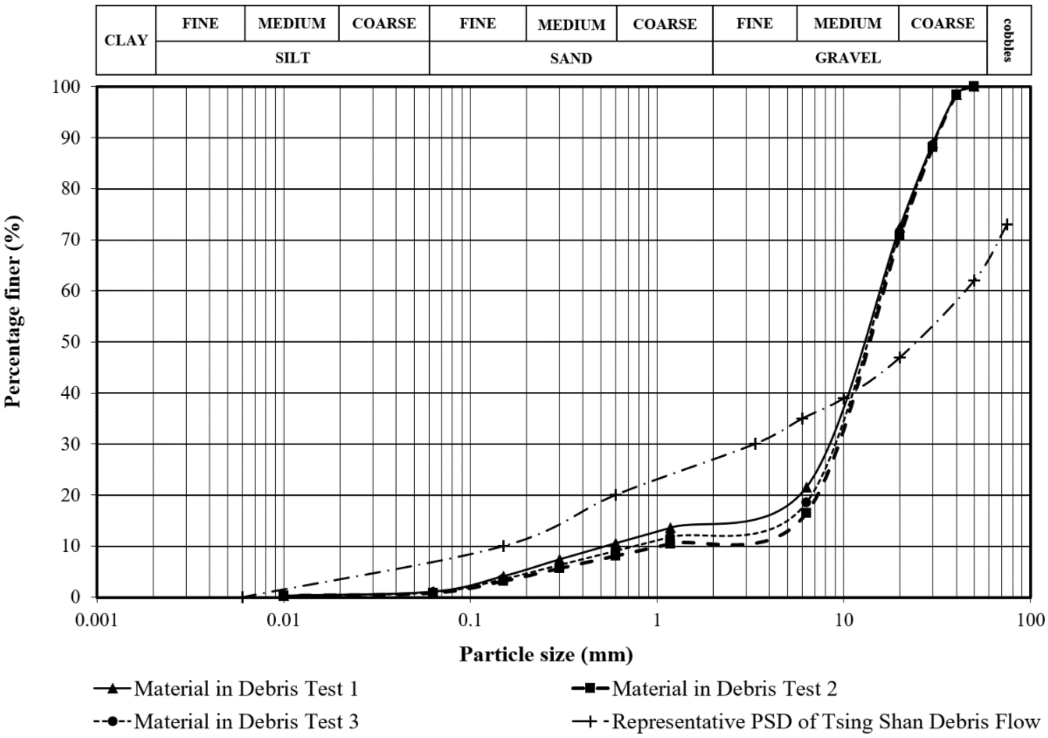

Figure 3. Particle Size Distribution (PSD) curves of the materials used in debris flow tests and the representative PSD of the Tsing Shan debris flow (King 2013)

(a)

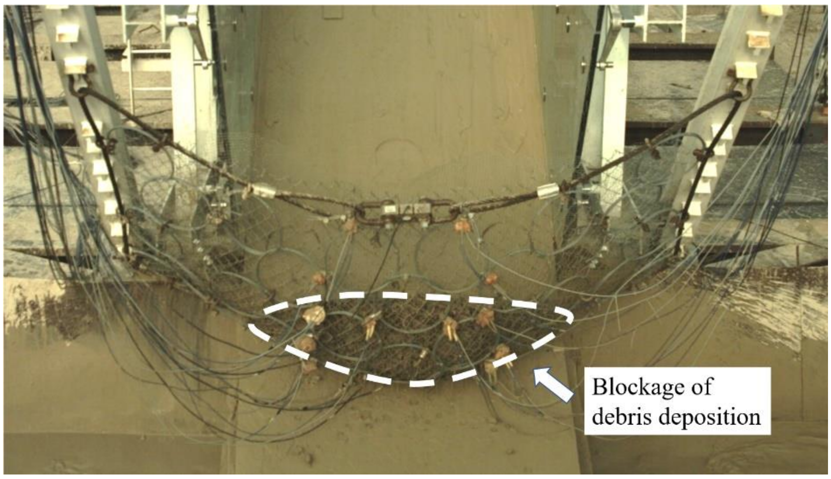

(b)

(c)

Figure 4. Blockage of the flexible barrier before (a) Debris Test 1, (b) Debris Test 2, and (c) Debris Test 3

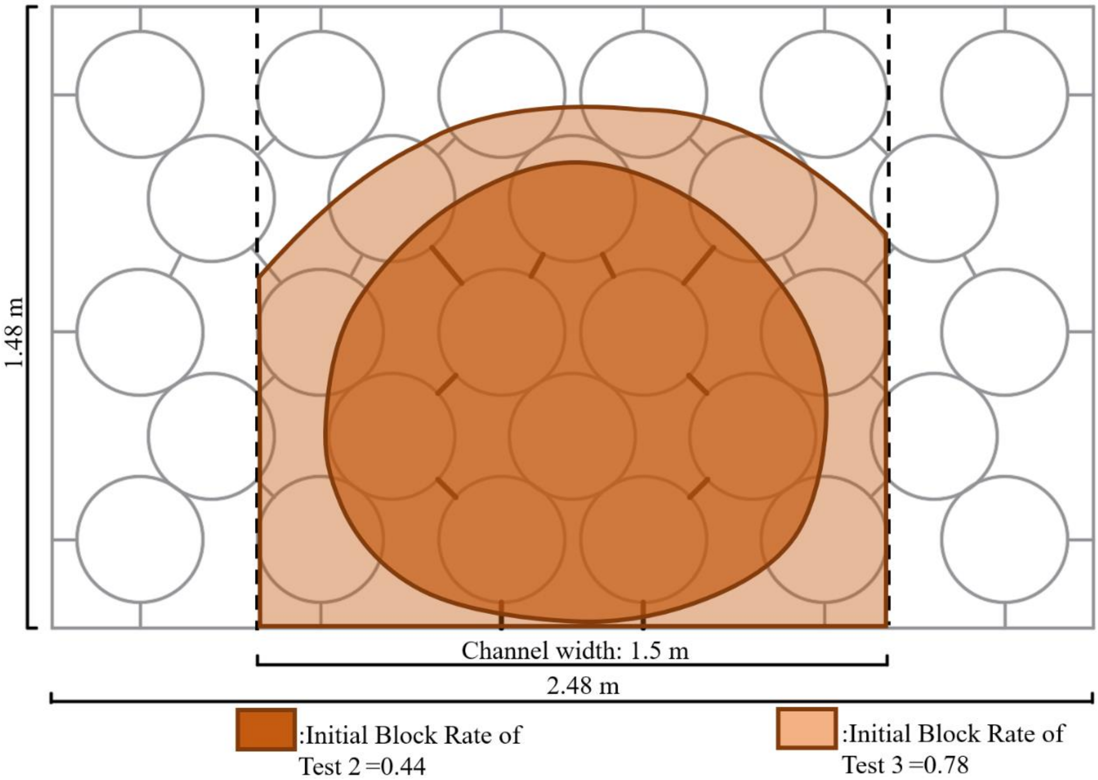

Figure 5. Initial blocked areas and the IBRs of Debris Test 2 and Debris Test 3

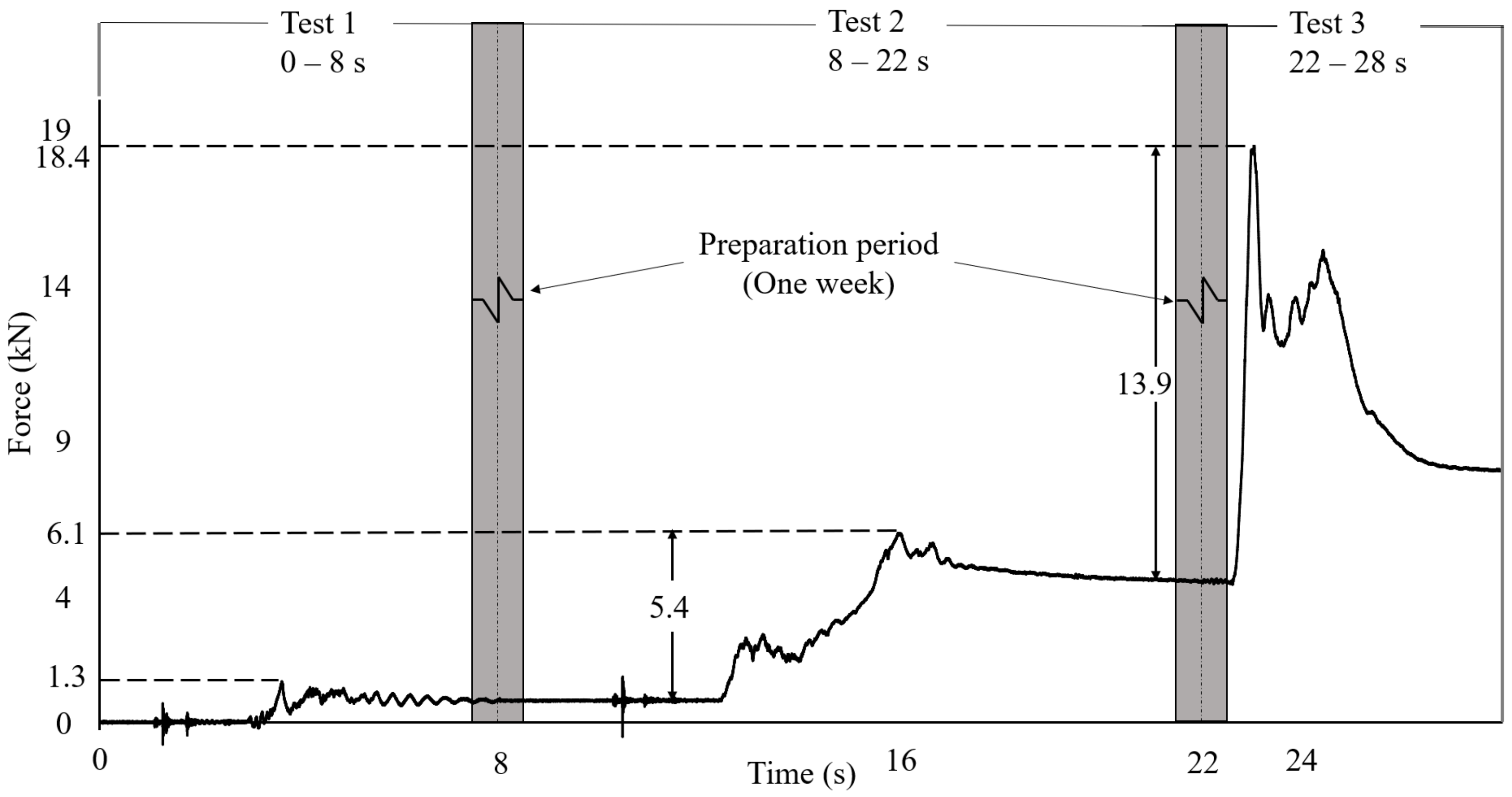

Figure 6. Impact force history on the supporting structures in Debris Tests 1, 2, and 3

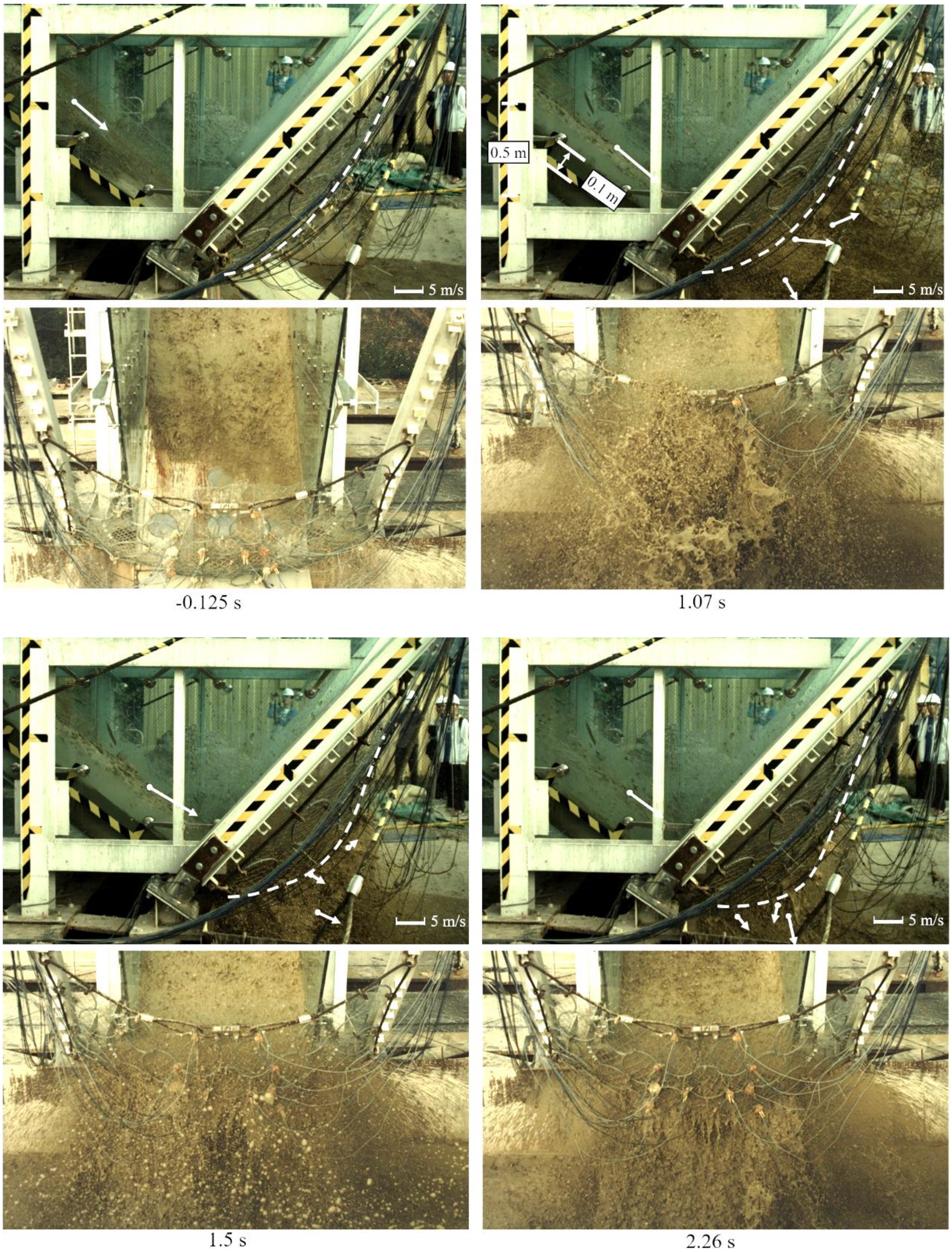

Figure 7. Side-front view photographs of the impact process in Debris Test 1 (IBR=0)

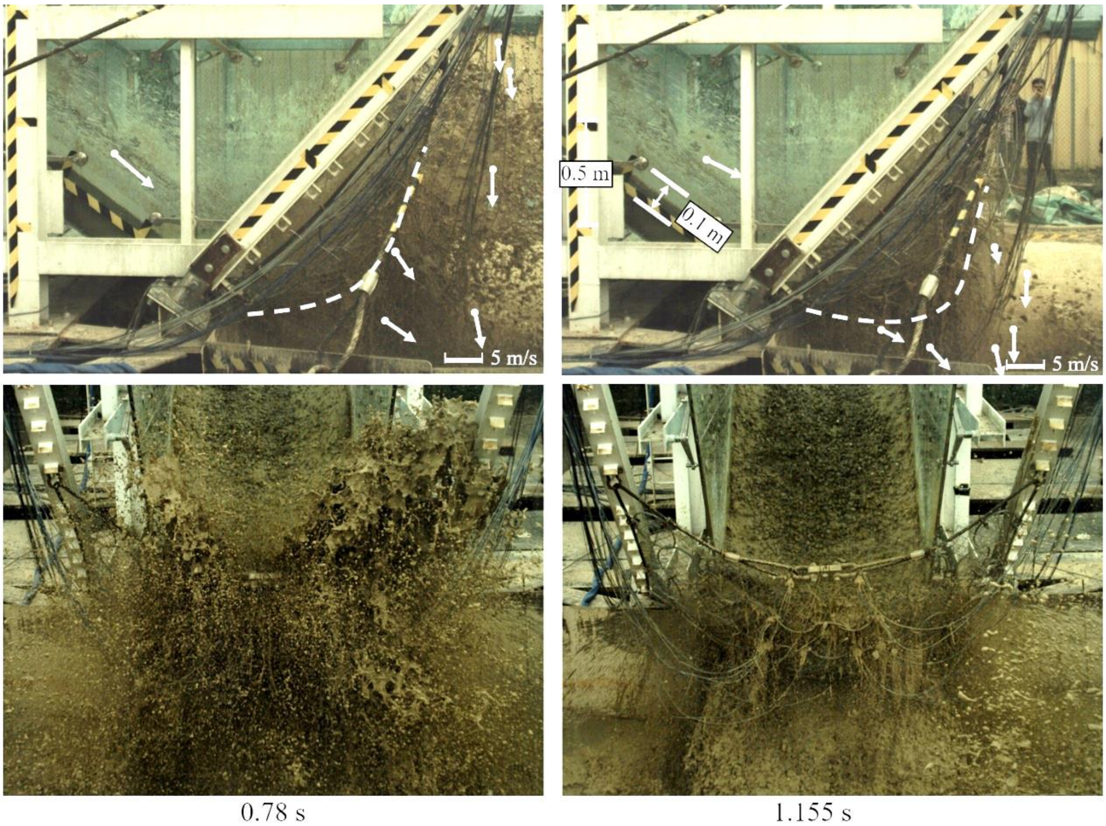

Figure 8. Side-front view photographs of the impact process in Debris Test 2 (IBR=0.44)

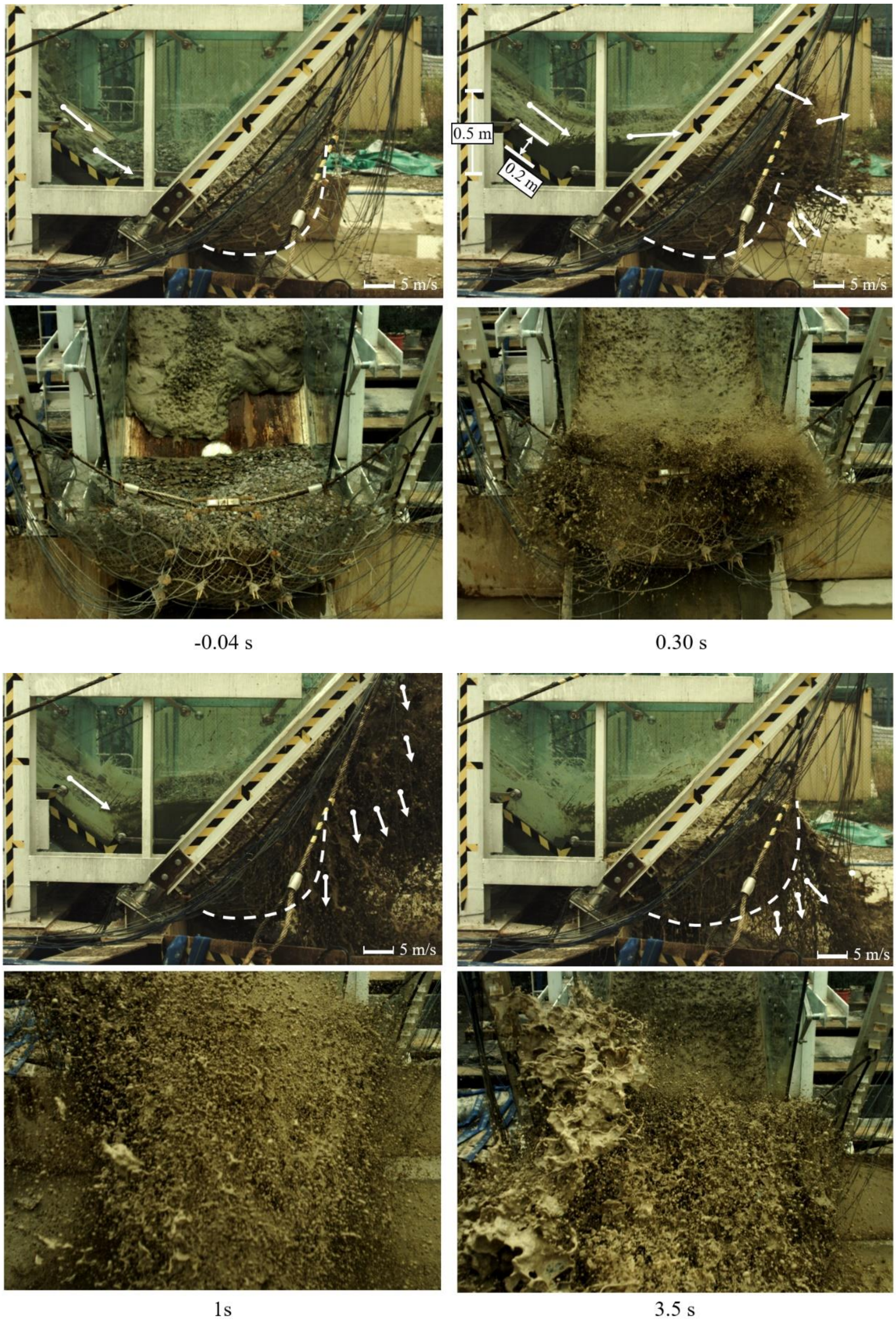

Figure 9. Side-front view photographs of the impact process in Debris Test 3 with IBR=0.78

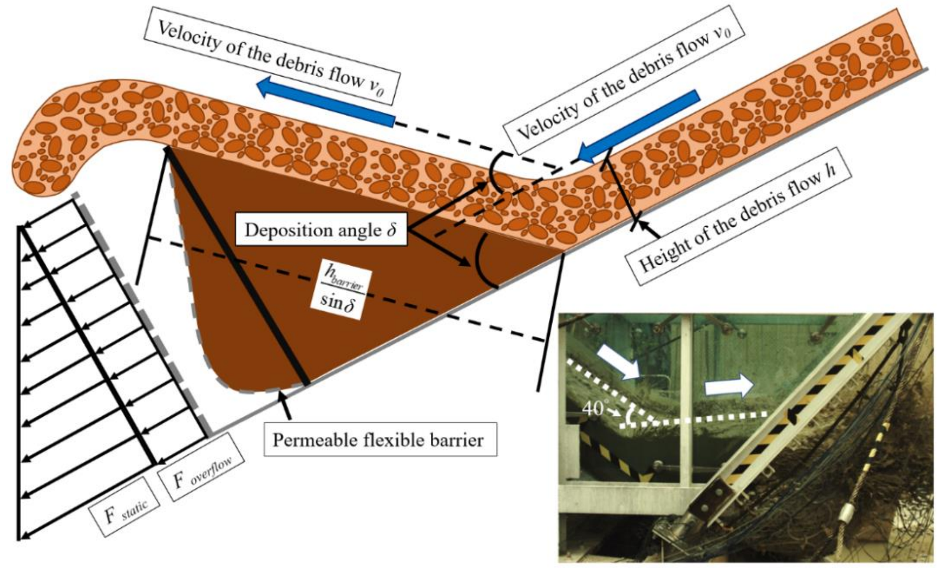

(a)

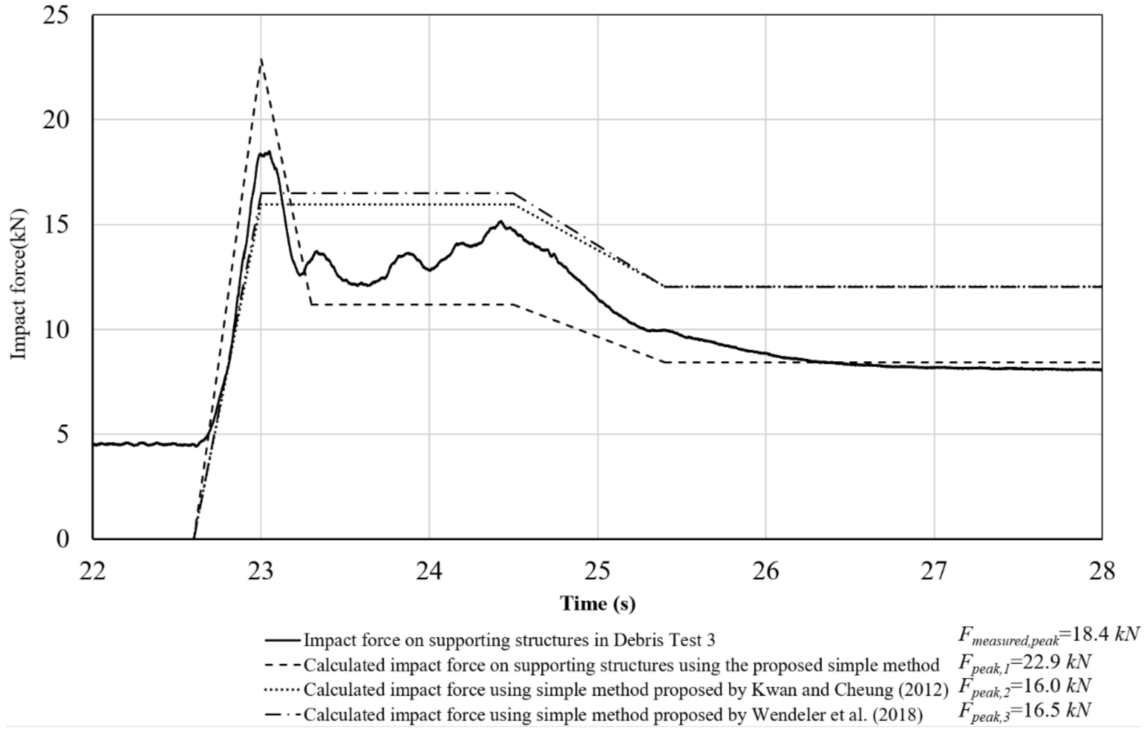

(b)

Figure 10. (a) Sketches of the overflow stage and (b) the comparison of the impact loading history on the supporting structures in the overflow stage with the calculated force combination using different simple methods

Table List:

Table 1. Parameters and measured values of the debris flow tests

Parameters	Multiple debris impact tests with overflow		
	Debris Test 1	Debris Test 2	Debris Test 3
Bulk density (kg/m^3)	1604	1811	1708
Water content (%)	89.4	50.5	67
Total volume of debris flow mixture (m^3)	2.00	2.30	2.28
Retained volume of debris flow mixture (m^3)	0.2	1.0	N/A (Overflowed)
Trapping ratio (%)	10	45	N/A (Overflowed)
Initial Block Rate (IBR)	0	0.44	0.78
Velocity before impact (m/s)	6.7	6.5	6.1
Flow depth (m)	0.1	0.1	0.2
$Fr = \frac{v_0}{\sqrt{gh}}$	6.76	6.56	4.36
Equivalent incremented maximum impact force on supporting structures (kN)	1.3	5.4	13.9

Table 2. Parameters for calculation of the impact force in the overflow stage

g (m/s^2)	$h_{barrier}$ (m)	w (m)	κ	ρ_{bulk} (kg/m^3)	ρ_d (kg/m^3)	v (m/s)	h (m)	ε (°)	φ (°)	ξ (m/s^2)
9.81	0.89	1.5	1	1708	2075	6.1	0.2	40	11	500

Table 3. Calculated forces on the supporting structures in the overflow stage using Eq.(13)

Type of force	Representative equation	Calculated force (kN)
$\boldsymbol{F_{instant,s}}$	$F_{instant,s} = (1-\beta)v_0^2 hw\rho_{bulk}(1-\cos\delta+\sin\delta)$	**11.7**
$\boldsymbol{F_{static,s}}$	$F_{static,s} = 0.5(1-\beta)\kappa\rho_d g\left(c_{reduced}h_{design}\right)^2 w$	**8.4**
$\boldsymbol{F_{drag,s}}$	$F_{drag,s} = (1-\beta)h\rho_{bulk}g\left[\tan\varphi+\frac{v_0^2}{h\xi}\right]\cdot\frac{c_{reduced}\cdot h_{design}\cdot w}{\sin\delta}$	**2.8**
$\boldsymbol{F_{impact,1,s}}$	$F_{impact,1,s} = F_{peak,s} + F_{instant,s} + F_{drag,s}$	**22.9**
$\boldsymbol{F_{impact,2,s}}$	$F_{impact,2,s} = F_{static,s} + F_{drag,s}$	**11.2**
$\boldsymbol{F_{impact,3,s}}$	$F_{impact,3,s} = F_{static,s}$	**8.4**